CTPS1 inhibition synergizes with replication stress signaling inhibition in *MYC*-amplified Group 3 medulloblastoma

Matthew R Hathaway[1], Katherine E Gadek[1], Hawa L Jagana[1], Isabella C Terrones[1], John M Hemenway[1], Aya Miyaki[1], Ashmitha Rajendran[1,2], Michael Meechan[1], Leonel Elena-Sanchez[1], Nicholas A Vitanza[1,3,4,8], Barbara S Slusher[5,6], Siobhan S Pattwell[1,3,7], Myron K Evans II[1,3,7,8]*

[1] Ben Towne Center for Childhood Cancer Research, Seattle Children's Research Institute, Seattle, WA, USA
[2] Biomedical Informatics and Medical Education Graduate Program, University of Washington, Seattle, WA, USA
[3] Department of Pediatrics, University of Washington School of Medicine, Seattle, WA, USA
[4] Clinical Research Division, Fred Hutchinson Cancer Center, Seattle, WA, USA
[5] Johns Hopkins Drug Discovery, Baltimore, MD, USA
[6] Department of Neurology, The Johns Hopkins University School of Medicine, Baltimore, MD, USA
[7] Human Biology Division, Fred Hutchinson Cancer Center, Seattle, WA, USA
[8] Department of Laboratory Medicine and Pathology, University of Washington School of Medicine, Seattle, WA, USA

* Address correspondence to:
Myron K Evans II, Ph.D.
Ben Towne Center for Childhood Cancer Research
1920 Terry Avenue
Seattle, WA 98101
Telephone: +1 206-884-4363
Email: myron.evansii@seattlechildrens.org

Keywords: CTPS1, medulloblastoma, MYC, glutamine, CHK1

Financial support: National Cancer Institute of the National Institutes of Health under Award Numbers K22CA262343 (MKE) and K22CA258953 (SSP), Kate Amato Foundation (MKE), Steven Higgins Brain Tumor Research Fund (MKE), Unravel Pediatric Cancer (MKE), Pediatric Brain Tumor Foundation (MKE), Seattle Children's Guild Association, and UW/FHCC/SCH Cancer Center Support Grant (P30CA015704).

Conflict of Interest

Author B.S.S. is an inventor of patent applications filed by Johns Hopkins Technology Ventures covering novel glutamine antagonists, including JHU083 and JHU395, and their utility which has been licensed to Dracen Pharmaceuticals. B.S.S. is also a co-founder and consultants for Dracen Pharmaceuticals. This arrangement has been reviewed and approved by Johns Hopkins University following their respective conflicts of interest policies.

N.A.V. serves as the scientific advisory board chair for BrainChild Bio, Inc. and is an inventor on issued and pending patents related to CAR T cell therapies. This arrangement has been reviewed and approved by Seattle Children's Research Institute following their respective conflicts of interest policies.

Abstract

MYC-driven medulloblastomas (MBs) represent the most aggressive and deadly subgroup of MB, the most common malignant pediatric tumor. Direct targeting of MYC itself remains an unmet clinical need, therefore focusing on vulnerabilities driven by MYC may be a viable option for novel therapeutic interventions. Using whole-genome CRISPR screening, we identified the *de novo* pyrimidine synthesis enzyme CTP synthase (*CTPS1*) as a strong dependency in *MYC*-driven MB. CTPS1 is the final and rate-limiting step in the *de novo* pyrimidine synthesis pathway. Targeted inhibition of CTPS1 leads to decreased tumor cell proliferation and markedly reduces MYC expression in G3 MB models. Mechanistically, we demonstrate that single agent CTPS1 inhibition activates the replication stress signaling pathway mediated by ATM-CHK2 and ATR-CHK1. Blockade of CHK1 kinase activity increases sensitivity to CTPS1 inhibition and significantly impedes heterotopic MB tumor growth. CTPS1 enzymatic activity requires the amino acid glutamine, therefore we inhibited CTPS1 using the glutamine antagonists, JHU083 and JHU395. These compounds are prodrugs of 6-diazo-5-oxo-L-norleucine (DON) which were developed to exhibit exquisite blood-brain barrier penetrability. Combining JHU083 and CHK1 inhibition demonstrates potent synergy against patient-derived MB xenografts *in vivo*. Our findings strongly suggest that combining *de novo* pyrimidine synthesis and ATR-CHK1 inhibitors is a promising treatment for *MYC*-driven MBs.

72 **Key Points**

73 - *CTPS1* is a unique vulnerability in MYC-driven medulloblastoma
74 - CTPS1 inhibition activates the ATR-CHK1 replication stress response pathway
75 for cell survival
76 - Blockade of CTPS1 enzymatic activity synergizes with CHK1 inhibition *in vitro*
77 and *in vivo*

78 **Importance of the Study**

79 MYC hyperactivation in tumors drives multiple anabolic processes which contribute to
80 tumor proliferation and aggressiveness in patients. We show that targeting *de novo*
81 pyrimidine synthesis (via CTPS1) limits tumor growth and targets MYC itself through a
82 feedback mechanism. CTPS1 inhibition potently combines with CHK1 blockade and
83 enhances disease control in both heterotopic and orthotopic models of medulloblastoma
84 (MB). Our results support the clinical evaluation of combined CTPS1 and CHK1
85 inhibition in patients with *MYC*-driven MB.

86 **Introduction**

87 Despite being the second most common oncological diagnosis, brain tumors are the
88 leading cause of cancer-related mortality in children[1]. Medulloblastoma (MB), the most
89 common malignant pediatric brain tumor, exhibits a complex genomic landscape with
90 diverse molecular subgroups which significantly impact clinical outcomes[2,3]. Recent
91 advances in genomic, epigenomic, and proteomic profiling have identified four subgroups
92 of MB: WNT, SHH, Group 3, and Group 4. Patients with Group 3 MB account for ~25-
93 30% of all diagnosed cases and have the poorest overall survival of all groups[2].

94 Dysregulation of the proto-oncogene MYC is a hallmark of G3 MB, with patients exhibiting
95 recurrent gene amplification and genomic fusions[4] or high MYC activity due to increased
96 protein stability[5]. Despite our understanding of MYC as a critical oncogene[6], no direct
97 targeted agents have been tested clinically in pediatric patients. This has led to motivation
98 towards synthetic lethality approaches, targeting vulnerabilities specifically driven by
99 MYC hyperactivation[7].

100 MYC supports cancer cell proliferation through numerous mechanisms, including rewiring
101 of cellular metabolism, by modulating anabolic processes to sustain the heightened
102 demands of rapidly dividing cells. Oncogenic MYC drives the upregulation of key
103 enzymes crucial to nucleotide biosynthesis, ensuring a robust supply of purine and
104 pyrimidine precursors needed for rapid tumor cell proliferation[8]. Simultaneously, MYC
105 promotes metabolic rewiring of glycolysis and the pentose phosphate pathway (PPP),
106 channeling resources toward nucleotide synthesis[8]. This dynamic interplay is a
107 characteristic feature of G3 MB[9,10]. Further, it underscores the significance of MYC in

108 tailoring cellular metabolism to meet the unique demands of oncogenesis, unveiling
109 potential vulnerabilities that could be harnessed for targeted therapeutic interventions.
110 Inhibition of nucleotide synthesis and metabolism effectively induces cell death and is
111 commonly exploited by various chemotherapeutics sometimes used in the treatment of
112 MB[11,12]. However, these treatments commonly yield side effects in patients, suggesting
113 that targeting tumor specific metabolism pathways could alleviate negative sequelae.
114 CTP synthase 1 (CTPS1), the rate limiting enzyme in the *de novo* synthesis of the
115 nucleotide CTP, is one such metabolic target[13,14]. CTPS1 has previously been shown as
116 a vulnerability in various adult solid and liquid tumors[15-17] and a small molecule inhibitor
117 of CTPS1 is currently in clinical trials (NCT05463263). Further, a recent paper linked MYC
118 expression to CTPS1 inhibitor sensitivity, demonstrating synthetic lethality in colorectal
119 cancer[18]. Low on-target, off-tumor toxicity of this molecule (and others like it) is due to
120 significant compensation by the homolog CTPS2 in most tissues, excluding the lymphoid
121 compartment post-infection[19,20].
122 In this study, using functional genomics and small molecule inhibition, we characterize
123 CTPS1 as a targetable vulnerability in G3 MB and identify MYC-amplified MB as
124 exquisitely dependent on *de novo* pyrimidine but not purine synthesis. Unlike
125 hematological malignancies, where CTPS1 inhibition alone significantly inhibits growth
126 and increases apoptosis[15,21], we observe limited cytotoxicity as a single agent in G3 MB.
127 We demonstrate that inhibition of CTPS1 in G3 MB activates the ATR-CHK1 replication
128 stress response, enhancing cell survival; dual antagonism of *de novo* pyrimidine
129 synthesis and CHK1 synergizes *in vitro* and *in vivo*. Finally, we demonstrate that a blood-
130 brain barrier penetrant inhibitor of nucleotide biosynthesis combines with CHK1 inhibition

131 increasing survival in an orthotopic model of MB. Our findings identify CTPS1 as a novel
132 target and demonstrate that this combinatorial approach may be a valid option to move
133 forward clinically for patients with G3 MB.

134 **Results**

135 **CTPS1 and the *de novo* pyrimidine synthesis pathway are dependencies in Group**
136 **3 medulloblastoma**

137 Functional genomics screens allow for unbiased identification of potentially druggable
138 vulnerabilities in tumors and have been utilized to guide pre-clinical work and clinical trials
139 in both adult and pediatric oncology. To evaluate dependencies specific to Group 3
140 medulloblastoma (MB), we first explored the Pediatric Cancer Dependency Map[22]. Our
141 analysis of 4 well-characterized G3 MB cell lines (D283, D341, D425, and D458) versus
142 all other pediatric entities, revealed CTP synthase 1 (*CTPS1*) as the third-strongest
143 dependency (defined by a negative CHRONOS score, **Figure 1A**). Comparing G3 MB to
144 only peds CNS tumors still reveals a strong dependency on *CTPS1* (**Figure S1A**),
145 suggesting a specific function in *MYC*-amplified MB. CTPS1 is the rate limiting enzyme
146 responsible for the glutamine-dependent conversion of uridine triphosphate (UTP) to
147 cytidine triphosphate (CTP), an essential step of the *de novo* pyrimidine synthesis
148 pathway[14] (**Figure 1B**). Further analysis revealed significant dependencies on other
149 enzymes in the *de novo* pyrimidine synthesis pathway including Carbamoyl-phosphate
150 synthetase 2, aspartate transcarbamylase, and dihydroorotase (*CAD*), Uridine
151 monophosphate synthase (UMPS), and Dihydroorotate dehydrogenase (*DHODH*) (G3
152 MB vs. all peds, **Figure 1C, S1B** G3MB vs. peds CNS). UMP-CMP kinase (*CMPK1*)
153 scores as a vulnerability, however, no difference is seen when compared to other pediatric
154 tumors. This is further validated by a recent publication which revealed DHODH as a
155 druggable target by CRISPR screening in another G3 MB cell line (SUMB002)[23]. Mining
156 of CRISPR screening data in two fetal neural stem cell (NSC) lines[24] shows no

157 dependency on *CTPS1* or other *de novo* pyrimidine synthesis enzyme genes (**Figure**
158 **S1C**). Interestingly, neither disruption of *CTPS2* (**Figure 1C, S1B**) or genes in the salvage
159 pathway (**Figure S1D**) had any effect on cell growth, suggesting a strong, non-redundant
160 role for *CTPS1* in G3 MB.

161 **Higher *CTPS1* expression is associated with disease advancement and poor**
162 **prognosis in MB**

163 Using a batch-normalized bulk RNA-seq resource (GSE124814)[25] comprised of 1350 MB
164 samples and 291 normal cerebellum revealed increased *CTPS1* expression in tumors
165 compared to normal cerebella (**Figure 1D**). Subgroup analysis uncovered the highest
166 average expression of *CTPS1* in G3 tumors in two independent datasets ($p<0.05$
167 G3vs.G4 and G3vs.SHH, **Figure 1E-F**). Analysis of a third dataset (GSE85217)[26] showed
168 a strong correlation between *MYC* and *CTPS1* expression in G3 MB tumors, with the
169 highest expression in those tumors characterized as Group3γ (**Figure 1G-H)**. *CTPS1*
170 expression also correlates with metastatic status of patients at time of diagnosis (**Figure**
171 **1I**), further demonstrating association with aggressive characteristics. We validated these
172 RNA-seq findings in a complementary proteomic dataset[5]. In this data, G3 MB tumors
173 were subclassified as G3a and G3b, where G3a tumors are characterized by a MYC-
174 activated state either by gene amplification or post-translational alterations which
175 increase MYC protein stability. We demonstrate higher CTPS1 protein levels in G3a vs.
176 G3b tumors (**Figure S1E**), as well as higher expression of other components of the *de*
177 *novo* pyrimidine pathway (**Figure S1F**). Immunohistochemistry of G3 MB patient-derived
178 xenografts confirm expression of CTPS1 in tumor tissue with little expression in normal
179 mouse tissue (**Figure 1J**). Weaker or no correlations were seen with other genes in the

180 pyrimidine synthesis pathway (**Figure S1G**). A correlation between *CTPS1* and *CCNB1*,
181 a key regulator of cell cycle progression and a proposed risk stratification gene[27], was
182 also noted (**Figure S1H**). Consistent with this, higher *CTPS1* expression was associated
183 with worse overall survival in all MB patients (**Figure 1K**) and in G3 MB patients with high
184 MYC expression (**Figure 1L**). Of the other *de novo* pyrimidine synthesis pathway
185 enzymes, only *DHODH* and *UMPS* expression correlated with poor survival in G3 MB
186 patients (**Figure S1I**).

187 **Targeting CTPS1 reduces MB cell proliferation *in vitro***

188 Based on the significant attenuation of growth using CRISPR-Cas9 targeting of *CTPS1*,
189 we targeted *CTPS1* using shRNA. After selection with puromycin, sphere formation was
190 assessed and cell proliferation measured by BrdU incorporation. In two different G3 MB
191 cell lines, cells exhibited decreased sphere forming capacity (**Figure 2A-B**), and
192 diminished proliferation concurrent with downregulation of *CTPS1* expression (**Figure**
193 **2C**). Despite significant growth inhibition *in vitro*, animals implanted with sh*CTPS1* cells
194 showed limited survival benefit compared to control shRNA implanted animals. HD-MB03
195 sh*CTPS1* tumors retained CTPS1 expression suggesting a negative selection for cells
196 with *CTPS1* knockdown *in vivo* (data not shown). We next employed treatment with 3-
197 Deazauridine (DAU) which is a structural analog of uridine that competitively inhibits the
198 synthesis of CTP by both CTPS1 and CTPS2[28]. DAU treatment caused a dose-dependent
199 decrease in cell proliferation (measured by CellTiter-Glo™) across a panel of G3 MB cell
200 lines (**Figure 2D**). This inhibition could be reversed by supplementation of either uridine
201 or cytidine, but not adenosine or guanosine (**Figure 2E**). Similar to previously published
202 data[16,29], CTPS1 pharmacological inhibition resulted in S-phase blockade with decreased

203 cells in G_0-G_1, which was reversed by addition of cyt or urid (**Figure 2F, S2A**).
204 Furthermore, DAU treatment also decreased MYC expression in tumor lines similar to
205 previous reports with DHODH inhibition in G3 MB[23,30] (**Figure 2G**).

206 **G3 MB cells are dependent on *de novo* pyrimidine but not *de novo* purine synthesis**

207 Previous work in other tumor types has revealed that MYC regulates both pyrimidine and
208 purine biosynthesis through direct regulation of multiple enzyme-encoding genes in both
209 pathways[8]. Analysis of previously published ChIP-seq data from two human G3 MB
210 tumors demonstrates significant MYC binding at the *CTPS1* promoter, with lower binding
211 at the *CTPS2* promoter correlating with gene expression[31] (**Figure S3A,B**). Analysis of
212 the same dataset from **Fig 1D**. revealed strong correlation between *MYC* and numerous
213 genes encoding enzymes in the *de novo* purine synthesis pathway (**Figure S3C**).
214 Exploration of DepMap data revealed that while some genes in the pathway scored as
215 dependencies, they were no different than pediatric CNS tumors (**Figure S3D**). The only
216 purine related enzyme that scores is thymidylate synthetase (TYMS), a catabolic one-
217 carbon metabolism enzyme that has an indirect effect on purine by driving thymidine
218 synthesis from dUMP salvage (**Figure S3E**). This correlates with activity of TYMS
219 inhibitors pemetrexed and 5-fluorouracil[32,33] and suggests the possibility of recently
220 developed novel inhibitors for future pre-clinical modeling[34,35].

221 To further clarify that inhibition of pyrimidine but not purine synthesis was antagonistic to
222 growth of G3 MB cells, we treated both Med-2112FHTC and Med-411FHTC with
223 lometrexol (LTX, GARFT inhibitor). We observed no effect on cell fitness after treatment
224 with LTX, similar to previous reports in IDH-mutant glioma and pediatric diffuse midline
225 glioma[36] (**Figure S3F**).

226 **CTPS1 inhibition alone is cytostatic but combines with CHK1 inhibition**

227 Western blot analysis of cells treated with DAU revealed little change in PARP cleavage,
228 a classic marker of apoptosis, at doses up to 5μM suggesting a cytostatic mechanism
229 rather than cytotoxicity (**Figure 3A**). Diehl et.al. recently published that nucleotide
230 imbalance, caused by targeting pyrimidine and/or purine enzymes, activates replication
231 stress signaling sensed by the ATR and ATM kinases[29]. These kinases sense both single-
232 and double- stranded breaks and phosphorylate CHK1 and CHK2, respectively, which
233 mediate survival and recovery of cells. We observed increased phosphorylation of both
234 CHK1 and CHK2 after treatment with DAU (**Figure 3B**). We then combined targeting of
235 CTPS1 with the potent CHK1/2 inhibitor prexasertib, which previously showed efficacy in
236 G3 MB cells[37]. Combining sublethal doses of prexasertib (**Figure S4A**) led to a dose-
237 dependent decrease in the IC_{50} of DAU in both HD-MB03 and Med-411FHTC cells
238 (**Figure 3C and D**). **Table 1** lists synergy scores as calculated by multiple reference
239 models[38] which revealed potent synergy between CTPS1 and CHK1/2 inhibition in G3
240 MB. This combination also led to apoptosis (**Figure 3C, inset** – cleaved PARP) and
241 significant DNA damage (measured by pH2AX) (**Figure 3E-F**). Prexasertib treatment also
242 synergized with BRQ, suggesting that CHK1 inhibition may broadly combine with
243 antagonism of *de novo* pyrimidine synthesis in G3 MB (**Figure S4B**). Utilizing a
244 heterotopic xenograft model of G3 MB in athymic nude mice, we assessed the efficacy of
245 combining DAU and prexasertib on tumor growth (**Figure 3G**). While single agent
246 targeting of either CTPS1 or CHK1 led to delays in tumor growth, the combination of DAU
247 and prexasertib synergized and completely abrogated growth in this model (**Figure 3H**).
248 Immunohistochemical analysis revealed decreased Ki67 corroborating our doubling time

249 findings (**Figure 3I**). Phosphorylation of H2AX was also elevated in combination treated
250 animals. Western blots revealed significant cleavage of PARP in our combination
251 treatment and sustained phosphorylation of CHK1/CHK2 (S345/S516) in combination
252 treatments (**Figure 3J**). We also noted decreased phosphorylation of the CHK1 target
253 CDC2 (Y15) in some combination treatment mice as well (data not shown).

254 **Targeted glutamine antagonism combines with CHK1 inhibition in orthotopic**
255 **models**

256 While our *in vitro* and *in vivo* data with DAU are striking, there is only one reference to
257 blood-brain barrier penetration of this compound in humans[39], tested in only a handful of
258 patients and never continued for clinical development. Interestingly, these adult patients
259 had intracerebral tumors which commonly have abnormally leaky vasculature[40]. MBs,
260 apart from the WNT subgroup, are characterized to have a fully intact BBB which
261 modulates response to BBB-impermeable drugs[41]. The combination of these make DAU
262 an unlikely candidate for G3 MB therapeutic development. CTPS enzymatic activity
263 requires the amino acid glutamine as well as ATP to produce CTP[42]. Glutamine is also
264 required at the first step of the *de novo* synthesis pathway catalyzed by CAD (**Figure 1B**).
265 Interestingly, the glutamine antagonist 6-diazo-5-oxo-l-norleucine (DON) was previously
266 shown to be an irreversible inhibitor of multiple nucleotide synthesis enzymes[43], including
267 CTPS1 and CAD. Single agent DON administration leads to significant phosphorylation
268 of CHK1/2 (**Figure 4A**) and cell death in G3 MB tumor cells (395 ref). We utilized two
269 prodrugs of DON – 1) isopropyl 6-diazo-5-oxo-2-(((phenyl (pivaloyloxy) methoxy) -
270 carbonyl) amino) hexanoate (JHU395) and 2) Ethyl 2-(2-Amino-4-methylpentanamido)-
271 DON (JHU083) – which exhibit enhanced lipophilicity and were previously shown to target

272 G3 MB tumor cells[44,45] (**Figure S5A**). We first tested JHU083 and JHU395 as single
273 agents in our patient-derived cell lines which revealed efficacy with inter-cell line variability
274 (**Figure 4B**). Co-administration of prexasertib synergized with both JHU083 (**Figure 4C**
275 **and D**) and JHU395 (**Figure 4E and F**), decreasing the IC_{50} in multiple G3 MB tumor
276 lines. Synergy analyses (**Table 1**) revealed stronger synergism of prexasertib with
277 JHU083 than with JHU395, so for the remainder of our study we used the combination of
278 JHU083+prexasertib. Combining JHU083 and prexasertib led to significant accumulation
279 of DNA damage (**Figure 4G-H**) similar to DAU+prexasertib. Previous work demonstrated
280 significant BBB penetration and tumor accumulation of both JHU083[44] and prexasertib[46]
281 in G3 MB tumor bearing mice, therefore we tested single agents and combinations after
282 orthotopic implantation of luciferase-expressing G3 MB cells. After confirmation of tumor
283 growth by IVIS imaging, mice were randomized to one of 4 groups and treated with
284 JHU083 alone or in combination with prexasertib (**Figure 4I**). While single agent
285 administration had limited effect on tumor growth or animal survival, the combination of
286 JHU083 and prexasertib significantly extended the median survival in animals implanted
287 with either HD-MB03 (**Figure 4J, S5B**) or Med-411FHTC (**Figure 4K, S5C**). Further, this
288 combination as well as our DAU+prexasertib combination had limited systemic toxicities
289 as measured by weight loss in animals (**Figure S5D,E**). Western immunoblot analysis of
290 tumors revealed increased phospho-CHK1/2 and phospho-CDC2 in JHU083 single agent
291 treated tumors. Combination treatment led to a blockade of CHK1/2 and CDC2
292 phosphorylation as well as a decrease in proliferation as measured by PCNA (**Figure 4L**).

293 **Discussion**

294 Herein, we report a dependency on *CTPS1* in *MYC*-amplified MBs when compared to
295 other pediatric malignancies. Interrogation of patient data revealed high expression of
296 *CTPS1* in tumors compared to normal brain with *MYC*-amplified G3γ tumors displaying
297 the highest expression. This was confirmed using recently published proteomics data
298 which correlates CTPS1 with G3a tumors, characterized by increased MYC expression
299 and activity[5]. Consistent with these findings, *CTPS1* expression correlates with poor
300 survival in *MYC* high patients. CTPS1, along with its homolog CTPS2, catalyze the rate
301 limiting step of the *de novo* pyrimidine biosynthesis pathway. Interestingly, *MYC*-amplified
302 MB tumors do not show a dependency on CTPS2, which also shows no correlation with
303 survival. This is consistent with previous reports that demonstrate differential activity of
304 the two enzymes, despite ~70% protein sequence homology[47]. Further analysis revealed
305 vulnerabilities to deletion of other members of the *de novo* pyrimidine biosynthesis
306 pathway, confirming previous reports of altered pyrimidine metabolism in MYC-amplified
307 MB[23], and more broadly across a number of other brain tumor types[36]. Furthermore,
308 recent work in a chemotherapy-resistant model of MB revealed upregulation of pyrimidine
309 metabolic processes in resistant tumors[48], suggesting utility of CTPS1 targeting in both
310 upfront and recurrence settings.

311 Using shRNAs and a small molecule inhibitor of CTPS1 (3-deazuridine, DAU) we
312 demonstrate that single agent targeting of CTPS1 leads to cell cycle arrest and decreased
313 proliferation which can be rescued by addition of exogenous pyrimidine nucleosides *in*
314 *vitro*. This targeting of CTPS1 also leads to a decrease in MYC expression which may
315 further impact tumor growth. Interestingly, germline mutations in *CTPS1* lead to no overt

316 phenotypes outside of the hematopoietic system, suggesting that inhibition may deliver
317 potent on-target effects in tumors while limiting deleterious side effects in patients[19,20].
318 This is highlighted by single agent efficacy of DAU in our flank model with no significant
319 weight loss observed. Mechanistically, amplified or hyperactive MYC in G3 MB induces
320 expression of CTPS1 required to synthesize nucleosides to maintain replicative capacity
321 of tumors. Inhibition of CTPS1 limits the pool of CTP available for replication[11], leading to
322 activation of the replication stress response pathway mediated by ATR-CHK1/ATM-CHK2
323 and subsequent cell cycle and proliferation arrest. Combined targeting of CTPS1 and the
324 replication stress pathway forces cells to continue through the cell cycle, accumulating
325 significant DNA damage and undergoing apoptosis (**Figure 5**).
326 This phenomenon has been observed in other tumor and normal cell types wherein
327 combining nucleotide depletion with ATR/ATM inhibitors leads to cell death[16,18,29]. We
328 demonstrate significant synergy between the CHK1 inhibitor, prexasertib, and DAU both
329 *in vitro* and *in vivo*. Further, we also demonstrate that the DHODH inhibitor, brequinar,
330 also synergizes with CHK1*i*, suggesting the utility of dual *de novo* pyrimidine synthesis
331 and replication stress signaling inhibition in treatment of *MYC*-amplified MB. Identification
332 of this combination may further enhance the clinical utility of a DHODH inhibitor from
333 Bayer which shows potent BBB penetration, but whose clinical development was halted
334 due to single agent inactivity (NCT03404726).
335 Excitingly, CTPS1 inhibitors have recently entered clinical development (NCT05463263)
336 for hematological malignancies, however blood-brain barrier (BBB) penetrance has not
337 been assessed. This compound (STP938) mimics CTP and acts an allosteric inhibitor of
338 enzymatic activity; impeding CTPS1 binding to UTP. CTPS1 also has a glutamine

339 amidotransferase domain which hydrolyzes glutamine to ammonia which is required for
340 catalysis of 4-phosphoryl UTP to CTP. Previous work identified that the glutamine
341 antagonist 6-Diazo-5-oxo-L-norleucine (DON) also binds to this domain, as well as other
342 glutamine utilizing enzymes, to inhibit covalent binding of glutamine[43]. We observed a
343 similar activation of CHK1/2 when cells were treated with DON as with DAU. While DON
344 does accumulate in mouse models of brain tumors, previous clinical trials were
345 unsuccessful due to dose-limiting toxicities[49]. We utilized two DON prodrugs, JHU083 and
346 JHU395, with enhanced BBB penetrability and offset of toxic side effects. These inhibitors
347 combine strongly with CHK1 inhibition *in vitro*, with the combination of JHU083 and
348 prexasertib showing significant synergy. We tested this combination *in vivo* and noted
349 increased survival, decreased proliferation, and increased apoptosis, and limited weight
350 loss despite prolonged combination treatment. While our studies are done in immune-
351 deficient models, recent studies have identified immune modulatory activity of
352 JHU083[50,51] which may bolster effects of this drug in immune-competent mouse models
353 and patients. Together, the data presented herein identify a targeted, combinatorial
354 approach for the treatment of *MYC*-amplified MB patients who currently have the least
355 favorable outcomes.

356 **Methods**

357 **Cell culture**

358 Patient derived medulloblastoma cell lines (Med-411FHTC and Med-2112FHTC, a gift
359 from J. Olson) were grown in NeuroCult NS-A Basal medium (Stemcell Technologies,
360 05750) with Neurocult NS-A Proliferation Supplement (Stemcell Technologies, 05753),
361 and 1% Penicillin/Streptomycin (Sigma-Aldrich, P4333). HD-MB03 (obtained from T.
362 Milde) and MB004 (a gift from P. Bandopadhayay) cell lines were grown in Gibco
363 Neurobasal medium (Gibco, 21-103-049) with 2% B27 Supplement (Gibco, 12587010),
364 1% N2 Supplement (Gibco, 21103049), 1% Glutamine (Gibco, 25030-81), 1%
365 Penicillin/Streptomycin (Sigma-Aldrich, P4333), and 1μg/mL Heparin (Stemcell
366 Technologies, 07980). All cell lines were grown as spheroids and media supplemented
367 with 0.2μg/mL each Human Epidermal Growth Factor Protein (Sino Biological, 10605-
368 HNAE-1) and Human Recombinant bFGF/FGF2 Protein (Sino Biological, 10014-HNAE-
369 1). HEK293T were obtained from American Type Culture collection and maintained in
370 DMEM (Gibco) with L-glutamine (Fisher Sci.), 10% fetal bovine serum (Fisher Sci.), 1%
371 L-Glutamine, and 1% Penicillin/Streptomycin (Sigma-Aldrich, P4333). All cells were
372 grown at 37°C and 5% CO_2.

373 **Drugs and small molecules**

374 3-Deazuridine (DAU) was obtained from Santa Cruz Biotechnology (394445) or Cayman
375 Chemical Company (23125). JHU395 and JHU083 were a gift from Barbara Slusher
376 (Johns Hopkins). Prexasertib mesylate (206787) and Prexasertib HCl (206989) were
377 procured from MedKoo Biosciences. Brequinar was procured from SelleckChem (S6626)
378 and Lometrexol from Cayman Chemical Company (18049). 6-diazo-5-oxo-L-nor-Leucine

379 (DON) was procured from Cayman Chemical Company (17580). Guanosine (S2439),
380 Adenosine (S1647), Cytidine (S2053), and Uridine (S2029) were procured from
381 SelleckChem. For *in vitro* use, drugs were reconstituted in DMSO (Millipore Sigma,
382 D2438).

383 **Proliferation measurements**

384 For Cell Titer Glo, cells were treated with serial concentrations of Prexasertib (0-20nM),
385 DAU (0-30nM), JHU083 (0-20μM), JHU395 (0-20μM), Lometrexol (0-180nM), and
386 Brequinar (0-180nM) or indicated combinations, then incubated for 72 hours. Proliferation
387 was assessed with CellTiter-Glo 2.0 (Promega, G9242) according to manufacturer
388 instructions and quantified using a Spectramax iD5. For BrdU assessment, cells
389 (untreated or treated as indicated) were incubated with 10μM BrdU (ThermoFisher,
390 B5002) for 1hr. After incubation, cells were rinsed with 1X PBS (Cytiva, BSS-PBS-1X6),
391 fixed in ice-cold 70% ethanol, and stored at -20°C. Fixed cells were washed with DPBS
392 and incubated in 2N HCl/0.5% Triton X-100 for 20 min. Cells were stained with anti-BrdU
393 FITC antibody (BioLegend, 364104) for 1 hour and analyzed on a BD Accuri C6 and
394 FlowJo (BD Biosciences).

395 **Cell cycle measurement**

396 For cell cycle measurement, cells were treated as indicated and fixed in ice-cold 70%
397 ethanol after PBS wash. FxCycle PI/RNase Staining Solution (ThermoFisher, F10797)
398 was added to cells as per manufacturer instruction. Analysis was performed on a BD
399 Accuri C6 and cell cycle analysis performed in FlowJo (BD Biosciences).

400 **Lentiviral shRNA production**

401 Lentiviral shRNA plasmids (U6 promoter) were designed and produced by Vectorbuilder.
402 shRNA sequences were:
403 shCTPS1: GCTCTCACATTACCTCCAGAA (TRCN0000045349)
404 shCTPS2: CGCCTCACCAAGGACAATAAT (TRCN0000369478)
405 HEK293T cells were plated on a 10cm dish (Corning, 877222) until 60-70% confluent.
406 Cells were transfected with 10μg transfer plasmid (VectorBuilder), 9μg psPAX2
407 (Addgene, 12260) and 3μg pMD2.G (Addgene, 12259) using Xfect Transfection Reagent
408 (Takara, 631318) according to manufacturer instructions. After transfection, virus was
409 collected in Neurobasal media, filtered through a 0.45μm syringe filter (Globe Scientific,
410 SF-PES-4530-S) and stored at -80°C. Viral particles were added to tumorspheres with
411 8μg/mL polybrene (Millipore Sigma, TR-1003-G) overnight. Forty-eight hours post-
412 infection, puromycin (Millipore Sigma, P4512-1MLX10) was added at 1μg/mL for 14 days
413 to select for infected cells.

414 **Western immunoblotting**

415 After indicated treatments, cells were lysed in RIPA buffer (150 mM NaCl; 50 mM Tris pH
416 8.0; 1.0% IGEPAL CA-630; 0.5% sodium deoxycholate; 0.1% SDS) (Thermo Scientific,
417 PI89900) with Halt protease and phosphatase inhibitor (Thermo Scientific, PI78445). For
418 tumor tissue, tissue was homogenized using an electric homogenizer fitted with a
419 disposable pestle in RIPA buffer. Protein was quantified using Pierce 660nm Protein
420 Assay Reagent (Thermo Scientific, 22660) and immunoblotted with standard procedures.
421 Antibodies and concentrations are listed Table S1.

422 **Immunofluorescence staining**

423 FFPE sections from flank tumors were deparaffinized and rehydrated with Histoclear
424 (HS2001, Fisher) and ethanol according to manufacturer instructions. Antigen retrieval
425 was performed by pressurized retrieval in pH 6.0 citrate buffer (C9999, Millipore Sigma)
426 for 5 min on high pressure in a pressure cooker (Cuisinart CPC-600 6 Quart 1000 Watt
427 Electric Pressure Cooker). Samples were blocked in 0.1% PBS+TX-100 5% donkey
428 serum (S30-M, Millipore Sigma) for 1 hr at RT prior to staining with antibodies overnight
429 at 4C. Secondary Alexa fluor antibodies (donkey anti-488, 555 or 647; Invitrogen) were
430 diluted at 1:500 in blocking buffer for 1 hour at RT. Samples were mounted in Prolong
431 Gold with NucBlue (P36981, Fisher Scientific). All samples were imaged on a Leica DMi8
432 microscope with Thunder deconvolution software (LAS X, Leica Microsystems) and
433 quantified in ImageJ.

434 **Synergy analysis**

435 Visualization and analysis of drug combinations were performed using the SynergyFinder
436 web application (version 3.0, https://synergyfinder.fimm.fi) using viability as readout.
437 Outlier detection was on with LL4 curve fitting. Bliss, ZIP, HSA, and Loewe scores and p-
438 values were calculated as described[38].

439 **Mouse xenograft experiments**

440 All animal procedures were approved by Institutional Animal Care and Use Committee
441 (IACUC) of Seattle Children's Research Institute (Protocol #00000675). Nude female
442 mice (Jackson Laboratories, NU:J- 002019 or 007850) were procured at 5 weeks of age
443 and allowed to acclimate for at least 1 week prior to cell implantation. Luciferase-
444 expressing cells were made by transduction of single cells with pLenti CMV mCherry-

445 T2A-Luc blast (a gift from N. Vitanza) followed by hand selection of positive tumorsphere
446 colonies.

447 ***Subcutaneous implantation***

448 Patient-derived MB cells were dissociated with Accutase (AT-104, Innovative Cell
449 Technologies), resuspended in Gibco Neurobasal Medium (21103049, Fisher Scientific),
450 and injected into the flank in a 100 μL aliquot containing 1.25×10^6 cells. Mice were
451 randomly segregated into groups when tumors reached 100 mm^3 volume: vehicle,
452 Prexasertib (10mg/kg subcutaneous twice daily), 3-Deazuridine (75mg/kg
453 intraperitoneal), or combination until health-defined end points. Tumor size was measured
454 with calipers. For growth curve analysis and survival studies, mice in study cohorts were
455 sacrificed when tumors reached a max of 3000 mm^3 in total volume. The tumors were
456 excised from sacrificed mice and subjected to routine histopathological processing.

457 ***Orthotopic implantation***

458 MB tumorspheres were treated with Accutase and approximately 100,000 mCherry-
459 positive cells injected per mouse in 2μL of sterile PBS (Cytiva, BSS-PBS-1X6). For
460 surgery, mice were given buprenorphine ER for analgesia and anesthetized with a
461 ketamine/xylazine mixture. A 0.9mm burr hole was made in the right cerebellum (-1.0mm
462 AP 1.0mm ML) from lambda and a stereotactic needle dispensed the cells in two 1μL
463 injections (2.5mm and 2.0mm DV) to deliver the cells. To monitor tumor growth, mice were
464 injected with 150 mg/kg of D-luciferin (LUCK-4G, Gold Biotechnologies), and imaged
465 using the IVIS Spectrum Imaging System 15 minutes post-injection.

466 ***In vivo* drug administration**

467 JHU083 was prepared in sterile PBS without Ca and Mg (Cytiva, BSSPBS1X6) and
468 administered at a concentration of 20mg/kg via oral gavage twice weekly. Prexasertib
469 mesylate (MEDKoo Biosciences, 206787) or prexasertib HCl (MEDKoo Biosciences,
470 206989) were prepared in 10% SBE-β-CD (MedChem Express, Cat# HY-17031/CS-
471 0731) and dosed at a concentration of 10mg/kg subcutaneously twice daily. 3-
472 Deazuridine (Santa Cruz Biotechnology, 394445) was diluted in corn oil (Millipore Sigma,
473 C8267-500ML) and dosed at a concentration of 75mg/kg IP once daily.

474 **Dependency Map Analysis**

475 Dependency data (CERES score) from the Broad Institute's Pediatric Cancer
476 Dependency Map[22] was accessed from the 23Q4 data deposit (depmap.org).

477 **Patient gene expression and proteomic analyses**

478 The processed expression of indicated genes were downloaded from the *R2: Genomics*
479 *Analysis and Visualization Platform* (**http://r2.amc.nl**) for indicated data sets[4,25,26]. When
480 calculating expression differences between different groups they were considered
481 significantly different when $P < 0.05$, as calculated using the one-way analysis of variance
482 (ANOVA) test included in the R2 online software. Linear regression was used to define
483 R-values and p-values for correlation plots. For significance of differences between
484 primary and metastatic tumors, the p-value was calculated with an unpaired
485 Student *t* test. For survival analyses in Kaplan–Meier plots, we used a 5-year/60-month
486 time point as a cut-off for survival due to the potential risk of including secondary tumors.
487 The *P* value for survival curves is calculated using a log-rank test of reported patient
488 survival data as described in R2 (**https://r2.amc.nl**). Only *a priori* fixed cut-offs (median

489 or top 1/3 v bottom 2/3) were used to calculate *P* values in the Kaplan–Meyer survival
490 analysis.
491 Proteomics data was downloaded from the Medulloblastoma Data Explorer
492 (https://medullo.shinyapps.io/archer2018/). One-way ANOVA was used to determine
493 significant differences.

494 **Acknowledgements**

495 We thank the University of Washington/Fred Hutchinson Cancer Center/Seattle
496 Children's Hospital Cancer Consortium for shared resources including Flow Cytometry
497 and Cell Sorting and Research Pathology supported by NCI P30CA015704. We thank
498 Virginia Hoglund and Galen Stewart for histopathology support, Jim Olson for providing
499 PDX tissue and cell lines, Beth Lawlor for reagent support, Karuna Patil and Rajesh
500 Utamanthil for animal husbandry and veterinary support. Research reported in this
501 manuscript was funded by the National Cancer Institute of the National Institutes of
502 Health under Award Numbers K22CA262343 (MKE) and K22CA258953 (SSP), Kate
503 Amato Foundation (MKE), Steven Higgins Brain Tumor Research Fund, Unravel
504 Pediatric Cancer, the Pediatric Brain Tumor Research Fund of Seattle Children's, the
505 Run of Hope Seattle, Seattle Children's Guild Association, and UW/FHCC/SCH Cancer
506 Center Support Grant (P30CA015704).

507

508 **Author contributions**

509 **Matthew R Hathaway:** Conceptualization, Data curation, Formal analysis,
510 Investigation, Methodology, Validation, Visualization, Writing – original draft, Writing –
511 review & editing. **Katherine E Gadek:** Data curation, Formal analysis, Investigation,

Methodology, Validation, Visualization, Software, Writing – original draft, Writing – review & editing. **Hawa L Jagana:** Data curation, Writing – review & editing. **Isabella C Terrones:** Data curation, Formal analysis, Writing – review & editing. **John M Hemenway:** Data curation, Formal analysis, Writing – review & editing. **Aya Miyaki:** Data curation, Writing – review & editing. **Ashmitha Rajendran:** Investigation, Writing – review & editing. **Michael Meechan:** Data curation, Investigation, Writing – review & editing. **Leonel Elena-Sanchez:** Data curation, Investigation, Writing – review & editing. **Nicholas A. Vitanza:** Methodology, Resources, Writing – review & editing. **Barbara S Slusher:** Methodology, Resources, Writing – review & editing. **Siobhan S Pattwell:** Methodology, Resources, Writing – review & editing. **Myron K Evans II:** Conceptualization, Funding acquisition, Methodology, Project administration, Software, Supervision, Validation, Writing – original draft, Writing – review & editing.

524 **Figure Legends**

525 **Figure 1: *CTPS1* is overexpressed in medulloblastoma and is a dependency in G3**
526 **MB. a,** Volcano plot comparing CERES scores of G3 MB cell lines (D283, D425, D458,
527 D341) versus other pediatric tumor lines (n=111) in the Dependency Map using two class
528 comparison. **b,** Diagram of *de novo* pyrimidine synthesis pathway, **c,** CERES gene
529 dependency scores for pyrimidine synthesis genes in G3 MB cells (n=4) compared to
530 other pediatric cell lines (n=111) in the DepMap, 23Q4 release. **d,** Quantile normalized
531 expression of CTPS1 in normal (n=291) or primary medulloblastoma (n=1350) samples.
532 **e-f,** Log_2 normalized expression of CTPS1 in GSEs (e-GSE124814, f-
533 EGAS00001001953). Samples are separated by MB subgroup. **g,** Linear regression of
534 log_2 normalized CTPS1 and MYC expression from GSE85217 separated by subtype. **h,**
535 Log_2 normalized expression of CTPS1 in G3 MB subtypes from same samples in **g**. **i,**
536 Log_2 normalized CTPS1 expression in primary tumor samples from patients with or
537 without metastases at diagnosis from GSE85217. **j,** Immunohistochemistry of G3 patient-
538 derived xenograft tissue after orthotopic implantation in nude mice (red-CTPS1, green-
539 human nuclear antigen (hNuc), blue-DNA). Scale bar=100 μM. **k,** Kaplan-Meier survival
540 of patients diagnosed with MB separated by median expression of *CTPS1*, GSE85217. **l,**
541 Kaplan-Meier survival of *Myc*-high G3 MB patients separated by top 1/3 versus bottom
542 2/3 expression of *CTPS1*. For **k** and **l**, number of patients are shown on inset. *, $P < 0.05$;
543 **, $P < 0.01$; ***, $P < 0.001$, Data are means ± SEM.

544 **Figure 2: CTPS inhibition suppresses cell proliferation in G3 MB tumor cells. a,**
545 Representative images of HD-MB03 tumorspheres transduced with indicated shRNAs
546 72h after plating. **b,** Quantification of area of tumorspheres formed in shScramble,

547 shCTPS1.1, and shCTPS1.2 transduced HD-MB03 cells. **c,** Quantification of FACS for
548 BrdU-positive HD-MB03 and MED-411FHTC cells transduced with indicated shRNAs
549 (n=3). *Inset*, Western immunoblot analysis of CTPS1 expression in transduced cells in **a-**
550 **c** Scr= scramble, 1.1 =shCTPS1.1, 1.2= shCTPS1.2. **d,** Cell proliferation analysis of HD-
551 MB03, MB004, Med-411FHTC, and Med-2112FHTC tumorspheres treated with indicated
552 concentrations of DAU for 72h. **e,** Cell proliferation analysis of HD-MB03 and Med-
553 411FHTC tumorspheres treated with vehicle or DAU (5μM) alone or in the presence of
554 50μM cytidine, uridine, adenosine, or guanine (n=3). **f,** Cell-cycle analysis of HD-MB03
555 cells treated with the indicated concentrations of DAU alone or in the presence of cytidine
556 (C) or uridine (U) for 48h (n=3). **g,** Western immunoblot analysis of MYC expression in
557 HD-MB03 cells treated with increasing doses of DAU. *, $P < 0.05$; **, $P < 0.01$; ***, $P <$
558 0.001, Data are means ± SEM.

559 **Figure 3: CTPS1 inhibition synergizes with ATR-CHK1 blockade *in vitro* and *in vivo*.**
560 Western immunoblot for **a,** PARP and **b,** phospho-CHK1/2 in Med-411FHTC or HD-MB03
561 cells treated with vehicle, 2.5μM, or 5μM DAU for 48h. **c,** Cell proliferation analysis of
562 Med-411FHTC (left) and HD-MB03 (right) tumorspheres with increasing concentrations
563 of DAU alone or in the presence of indicated prexasertib (CHK1 inhibitor) concentrations
564 (n=3). *Inset*, Western immunoblot analysis of cleaved PARP in cells treated with
565 prexasertib alone (1.25nM), DAU alone (2.5μM), or the combination. **d,** 2D contour plots
566 of synergy (Bliss calculation) between DAU and prexasertib in Med-411FHTC (left) and
567 HD-MB03 (right) tumorspheres calculated by Synergy Finder. **e,** Immunofluorescence for
568 phospho-H2AX in D283 G3 MB cells treated as indicated. Scale bar 25 μM. **f,**
569 Quantification of images in **e** (n=5 images per condition, experiment repeated twice). **g,**

570 Pre-clinical mouse treatment protocol for data shown in **h**. **h,** left – Tumor volume of HD-
571 MB03 flank xenografts treated as indicated n=5 (vehicle) or 6 (all others). Tumor volume
572 statistics (p-value) – veh-prex: 3.9E-6, veh-combo: 3.1E-11, prex-combo: 8.7E-3. TGI:
573 tumor growth inhibition DT: doubling time; right – Quantification of tumor weights in grams
574 at Day 20 post-treatment (veh, n=2, DAU, n=3, prex, n=3, combo, n=5). **i,** Representative
575 images of immunohistochemistry for Ki-67 and phospho-H2AX in tumors at endpoint. **j,**
576 Western immunoblot for total PARP (* denotes cleaved PARP) and phospho-CHK1/2 in
577 tumors from **h,**. *, P < 0.05; **, P < 0.01; ***, P < 0.001, Data are means ± SEM.

578 **Figure 4: CTPS1 inhibition via glutamine analogs synergizes with CHK1 inhibition**
579 **in orthotopic G3 MB models. a,** Western immunoblot for phospho-CHK1/2 in Med-
580 411FHTC (left) and HD-MB03 (right) tumorspheres treated with 10μM DON. **b,** Cell
581 proliferation analysis of HD-MB03, MB004, Med-411FHTC, and Med-2112FHTC
582 tumorspheres treated with indicated concentrations of JHU083 (left) and JHU395 (right)
583 for 72h (n=3). Cell proliferation analysis and 2D contour plots of synergy (Bliss calculation)
584 for **c, d** JHU083 and **e, f** JHU395 alone or in the presence of indicated prexasertib
585 concentrations (n=3). **g,** Immunofluorescence for phospho-H2AX in D283 G3 MB cells
586 treated as indicated. Scale bar 25 μM. **h,** Quantification of images in **g** (n=5 images per
587 condition, experiment repeated twice). **i,** Pre-clinical mouse treatment protocol for data
588 shown in **j-k**. Kaplan-Meier survival of mice orthotopically implanted with **j,** HD-MB03 or
589 **k,** Med-411FHTC cells transduced with luciferase expressing construct and treated as
590 indicated. **l,** Western immunoblot for phospho-CHK1/2, phospho-CDC2, and PCNA in
591 tumors from **j-k**. *, P < 0.05; **, P < 0.01; ***, P < 0.001, Data are means ± SEM.

592 **Figure S1: Dependency, gene expression and survival data for additional de *novo***
593 **pyrimidine synthesis and salvage pathway genes in G3 MB. a,** Volcano plot
594 comparing CERES scores of G3 MB cell lines (D283, D425, D458, D341) versus other
595 pediatric CNS tumor lines (n=17) in the Dependency Map using two class comparison. **b,**
596 CERES gene dependency scores for pyrimidine synthesis genes in G3 MB cells (n=4)
597 compared to other pediatric CNS tumor lines (n=17) in the DepMap, 23Q4 release. **c**,
598 CERES scores for normal NSCs (CB660 and U5) for *de novo* pyrimidine synthesis genes
599 as well as *TOP2A* and *RPA2* (controls). **d**, CERES gene dependency scores for
600 pyrimidine salvage genes in G3 MB cells (n=4) compared to all pediatric (left, n=111) and
601 peds CNS (right, n=17). **e**, Relative CTPS1 protein expression in G3a (n=8) and G3b
602 (n=6) tumors from(ref). **f**, Heatmap of relative protein expression for other *de novo*
603 pyrimidine synthesis proteins. **g**, Linear regression of $\log_2$ normalized *MYC* and *de novo*
604 pyrimidine synthesis gene expression from GSE85217 separated by subtype. **h**, Linear
605 regression of $\log_2$ normalized *CTPS1* and *CCNB1* expression separated by G3 subtype.
606 **i**, Kaplan-Meier survival of *MYC*-high G3 MB patients separated by top 1/3 versus bottom
607 2/3 expression of indicated genes. Number of patients are shown on inset.
608 **Figure S2: DAU treatment alters cell cycle in G3 MB. a,** Cell-cycle analysis of Med-
609 411FHTC cells treated with the indicated concentrations of DAU alone or in the presence
610 of cytidine (C) or uridine (U) for 48h (n=3). *, $P < 0.05$; **, $P < 0.01$; ***, $P < 0.001$, Data
611 are means ± SEM.
612 **Figure S3: MYC drives expression of pyrimidine and purine synthesis genes, but**
613 **G3 MB cells are insensitive to purine synthesis inhibition. a,** Representative ChIP-
614 sequencing tracks for MYC in human G3 MB cells at *CTPS1* and *CTPS2* promoters. **b,**

615 Expression (transcripts per million, TPM) of *CTPS1* and *CTPS2* in tumor samples from **a**.
616 **c,** Linear regression of log_2 normalized *MYC* and *de novo* purine synthesis gene
617 expression in G3 tumors. **d**, CERES gene dependency scores for *de novo* purine
618 synthesis genes in G3 MB cells (n=4) compared to peds CNS (n=17) cell lines. **e**, left -
619 CERES scores for *TYMS* in G3 MB (n=4), all peds (n=111), and peds CNS (n=17); right
620 - Linear regression of log_2 normalized *MYC* and *TYMS* expression in G3 tumors. **f**, Cell
621 proliferation analysis of Med-411FHTC and Med-2112FHTC tumorspheres treated with
622 indicated concentrations of lometrexol (LTX) for 72h (n=3). *, $P < 0.05$; **, $P < 0.01$; ***, P
623 < 0.001, Data are means ± SEM.

624 **Figure S4: Prexasertib alone has limited effect but synergizes with DHODH**
625 **inhibition.** Cell proliferation analysis of HD-MB03 and Med-411FHTC tumorspheres
626 treated with increasing concentrations of **a,** prexasertib alone or **b,** brequinar in the
627 presence of indicated doses of prexasertib. Data are means ± SEM.

628 **Figure S5: JHU083+prexasertib combination limits tumor growth in vivo. a,**
629 chemical structures of DON, JHU083, and JHU395. IVIS imaging of mice orthotopically
630 implanted with **b,** HD-MB03 or **c,** Med-411FHTC -luciferase expressing tumor lines
631 treated as indicated. Images are from mid-point of treatment. Monitored weights of
632 animals from **d,** heterotopic model treated with DAU and/or prexasertib and **e,** orthotopic
633 model treated with JHU083 and/or prexasertib.

634

635 **1.** Siegel DA, Richardson LC, Henley SJ, et al. Pediatric cancer mortality and survival in the
636 United States, 2001-2016. *Cancer.* 2020; 126(19):4379-4389.
637 **2.** Juraschka K, Taylor MD. Medulloblastoma in the age of molecular subgroups: a review. *J*
638 *Neurosurg Pediatr.* 2019; 24(4):353-363.
639 **3.** Shih DJ, Northcott PA, Remke M, et al. Cytogenetic prognostication within
640 medulloblastoma subgroups. *Journal of clinical oncology.* 2014; 32(9):886-896.

641 **4.** Northcott PA, Shih DJ, Peacock J, et al. Subgroup-specific structural variation across 1,000
642 medulloblastoma genomes. *Nature.* 2012; 488(7409):49-56.
643 **5.** Archer TC, Ehrenberger T, Mundt F, et al. Proteomics, Post-translational Modifications, and
644 Integrative Analyses Reveal Molecular Heterogeneity within Medulloblastoma Subgroups.
645 *Cancer Cell.* 2018; 34(3):396-410.e398.
646 **6.** Conacci-Sorrell M, McFerrin L, Eisenman RN. An overview of MYC and its interactome.
647 *Cold Spring Harb Perspect Med.* 2014; 4(1):a014357.
648 **7.** Wang C, Zhang J, Yin J, et al. Alternative approaches to target Myc for cancer treatment.
649 *Signal Transduction and Targeted Therapy.* 2021; 6(1):117.
650 **8.** Dong Y, Tu R, Liu H, Qing G. Regulation of cancer cell metabolism: oncogenic MYC in the
651 driver's seat. *Signal Transduction and Targeted Therapy.* 2020; 5(1):124.
652 **9.** Pham K, Hanaford AR, Poore BA, et al. Comprehensive Metabolic Profiling of MYC-
653 Amplified Medulloblastoma Tumors Reveals Key Dependencies on Amino Acid,
654 Tricarboxylic Acid and Hexosamine Pathways. *Cancers (Basel).* 2022; 14(5).
655 **10.** Tech K, Gershon TR. Energy metabolism in neurodevelopment and medulloblastoma.
656 *Transl Pediatr.* 2015; 4(1):12-19.
657 **11.** Parker WB. Enzymology of purine and pyrimidine antimetabolites used in the treatment
658 of cancer. *Chem Rev.* 2009; 109(7):2880-2893.
659 **12.** Shelton J, Lu X, Hollenbaugh JA, Cho JH, Amblard F, Schinazi RF. Metabolism, Biochemical
660 Actions, and Chemical Synthesis of Anticancer Nucleosides, Nucleotides, and Base
661 Analogs. *Chem Rev.* 2016; 116(23):14379-14455.
662 **13.** Huang M, Graves LM. De novo synthesis of pyrimidine nucleotides; emerging interfaces
663 with signal transduction pathways. *Cell Mol Life Sci.* 2003; 60(2):321-336.
664 **14.** Levitzki A, Koshland DE, Jr. Cytidine triphosphate synthetase. Covalent intermediates and
665 mechanisms of action. *Biochemistry.* 1971; 10(18):3365-3371.
666 **15.** Asnagli H, Minet N, Pfeiffer C, et al. CTP Synthase 1 Is a Novel Therapeutic Target in
667 Lymphoma. *Hemasphere.* 2023; 7(4):e864.
668 **16.** Pfeiffer C, Grandits AM, Asnagli H, et al. CTPS1 is a novel therapeutic target in multiple
669 myeloma which synergizes with inhibition of CHEK1, ATR or WEE1. *Leukemia.* 2024;
670 38(1):181-192.
671 **17.** Wu F, Mao Y, Ma T, et al. CTPS1 inhibition suppresses proliferation and migration in
672 colorectal cancer cells. *Cell Cycle.* 2022; 21(24):2563-2574.
673 **18.** Sun Z, Zhang Z, Wang Q-Q, Liu J-L. Combined Inactivation of CTPS1 and ATR Is Synthetically
674 Lethal to MYC-Overexpressing Cancer Cells. *Cancer Research.* 2022; 82(6):1013-1024.
675 **19.** Martin E, Minet N, Boschat AC, et al. Impaired lymphocyte function and differentiation in
676 CTPS1-deficient patients result from a hypomorphic homozygous mutation. *JCI Insight.*
677 2020; 5(5).
678 **20.** Martin E, Palmic N, Sanquer S, et al. CTP synthase 1 deficiency in humans reveals its central
679 role in lymphocyte proliferation. *Nature.* 2014; 510(7504):288-292.
680 **21.** Durand R, Bellanger C, Kervoëlen C, et al. Selective pharmacologic targeting of CTPS1
681 shows single-agent activity and synergizes with BCL2 inhibition in aggressive mantle cell
682 lymphoma. *Haematologica.* 2024.
683 **22.** Dharia NV, Kugener G, Guenther LM, et al. A first-generation pediatric cancer dependency
684 map. *Nat Genet.* 2021; 53(4):529-538.

685 **23.** Gwynne WD, Suk Y, Custers S, et al. Cancer-selective metabolic vulnerabilities in MYC-
686 amplified medulloblastoma. *Cancer Cell.* 2022; 40(12):1488-1502.e1487.
687 **24.** O'Connor SA, Feldman HM, Arora S, et al. Neural G0: a quiescent-like state found in
688 neuroepithelial-derived cells and glioma. *Mol Syst Biol.* 2021; 17(6):e9522.
689 **25.** Weishaupt H, Johansson P, Sundström A, et al. Batch-normalization of cerebellar and
690 medulloblastoma gene expression datasets utilizing empirically defined negative control
691 genes. *Bioinformatics.* 2019; 35(18):3357-3364.
692 **26.** Cavalli FMG, Remke M, Rampasek L, et al. Intertumoral Heterogeneity within
693 Medulloblastoma Subgroups. *Cancer Cell.* 2017; 31(6):737-754.e736.
694 **27.** de Haas T, Hasselt N, Troost D, et al. Molecular risk stratification of medulloblastoma
695 patients based on immunohistochemical analysis of MYC, LDHB, and CCNB1 expression.
696 *Clin Cancer Res.* 2008; 14(13):4154-4160.
697 **28.** McPartland RP, Wang MC, Bloch A, Weinfeld H. Cytidine 5'-triphosphate synthetase as a
698 target for inhibition by the antitumor agent 3-deazauridine. *Cancer Res.* 1974;
699 34(11):3107-3111.
700 **29.** Diehl FF, Miettinen TP, Elbashir R, et al. Nucleotide imbalance decouples cell growth from
701 cell proliferation. *Nat Cell Biol.* 2022; 24(8):1252-1264.
702 **30.** Dorasamy MS, Choudhary B, Nellore K, Subramanya H, Wong PF. Dihydroorotate
703 dehydrogenase Inhibitors Target c-Myc and Arrest Melanoma, Myeloma and Lymphoma
704 cells at S-phase. *J Cancer.* 2017; 8(15):3086-3098.
705 **31.** Ecker J, Thatikonda V, Sigismondo G, et al. Reduced chromatin binding of MYC is a key
706 effect of HDAC inhibition in MYC amplified medulloblastoma. *Neuro Oncol.* 2021;
707 23(2):226-239.
708 **32.** Morfouace M, Shelat A, Jacus M, et al. Pemetrexed and Gemcitabine as Combination
709 Therapy for the Treatment of Group3 Medulloblastoma. *Cancer Cell.* 2014; 25(4):516-529.
710 **33.** Morrison LC, McClelland R, Aiken C, et al. Deconstruction of medulloblastoma cellular
711 heterogeneity reveals differences between the most highly invasive and self-renewing
712 phenotypes. *Neoplasia.* 2013; 15(4):384-398.
713 **34.** Costantino L, Ferrari S, Santucci M, et al. Destabilizers of the thymidylate synthase
714 homodimer accelerate its proteasomal degradation and inhibit cancer growth. *Elife.* 2022;
715 11.
716 **35.** Guijarro MV, Kellish PC, Dib PE, et al. First-in-class multifunctional TYMS nonclassical
717 antifolate inhibitor with potent in vivo activity that prolongs survival. *JCI Insight.* 2023;
718 8(10).
719 **36.** Schild T, Keshari KR. Revealing de novo pyrimidine synthesis as a key vulnerability in brain
720 tumors. *Cancer Cell.* 2022; 40(12):1457-1458.
721 **37.** Endersby R, Whitehouse J, Pribnow A, et al. Small-molecule screen reveals synergy of cell
722 cycle checkpoint kinase inhibitors with DNA-damaging chemotherapies in
723 medulloblastoma. *Science Translational Medicine.* 2021; 13(577):eaba7401.
724 **38.** Ianevski A, Giri AK, Aittokallio T. SynergyFinder 3.0: an interactive analysis and consensus
725 interpretation of multi-drug synergies across multiple samples. *Nucleic Acids Research.*
726 2022; 50(W1):W739-W743.

39. Stewart DJ, Benvenuto JA, Leavens M, et al. Penetration of 3-Deazauridine into Human Brain, Intracerebral Tumor, and Cerebrospinal Fluid1. *Cancer Research.* 1979; 39(10):4119-4122.

40. Hirano A, Matsui T. Vascular structures in brain tumors. *Hum Pathol.* 1975; 6(5):611-621.

41. Phoenix TN, Patmore DM, Boop S, et al. Medulloblastoma Genotype Dictates Blood Brain Barrier Phenotype. *Cancer Cell.* 2016; 29(4):508-522.

42. Weng ML, Zalkin H. Structural role for a conserved region in the CTP synthetase glutamine amide transfer domain. *J Bacteriol.* 1987; 169(7):3023-3028.

43. Ortlund E, Lacount MW, Lewinski K, Lebioda L. Reactions of Pseudomonas 7A glutaminase-asparaginase with diazo analogues of glutamine and asparagine result in unexpected covalent inhibitions and suggests an unusual catalytic triad Thr-Tyr-Glu. *Biochemistry.* 2000; 39(6):1199-1204.

44. Hanaford AR, Alt J, Rais R, et al. Orally bioavailable glutamine antagonist prodrug JHU-083 penetrates mouse brain and suppresses the growth of MYC-driven medulloblastoma. *Transl Oncol.* 2019; 12(10):1314-1322.

45. Pham K, Maxwell MJ, Sweeney H, et al. Novel Glutamine Antagonist JHU395 Suppresses MYC-Driven Medulloblastoma Growth and Induces Apoptosis. *J Neuropathol Exp Neurol.* 2021; 80(4):336-344.

46. Campagne O, Davis A, Maharaj AR, et al. CNS penetration and pharmacodynamics of the CHK1 inhibitor prexasertib in a mouse Group 3 medulloblastoma model. *Eur J Pharm Sci.* 2020; 142:105106.

47. Minet N, Boschat AC, Lane R, et al. Differential roles of CTP synthetases CTPS1 and CTPS2 in cell proliferation. *Life Sci Alliance.* 2023; 6(9).

48. Mariotto E, Rampazzo E, Bortolozzi R, et al. Molecular and functional profiling of chemotolerant cells unveils nucleoside metabolism-dependent vulnerabilities in medulloblastoma. *Acta Neuropathol Commun.* 2023; 11(1):183.

49. Lemberg KM, Vornov JJ, Rais R, Slusher BS. We're Not "DON" Yet: Optimal Dosing and Prodrug Delivery of 6-Diazo-5-oxo-L-norleucine. *Mol Cancer Ther.* 2018; 17(9):1824-1832.

50. Lee K, Thompson EA, Gharaie S, et al. T cell metabolic reprogramming in acute kidney injury and protection by glutamine blockade. *JCI Insight.* 2023; 8(12).

51. Praharaj M, Shen F, Lee AJ, et al. Metabolic reprogramming of tumor-associated macrophages using glutamine antagonist JHU083 drives tumor immunity in myeloid-rich prostate and bladder cancer tumors. *Cancer Immunol Res.* 2024.

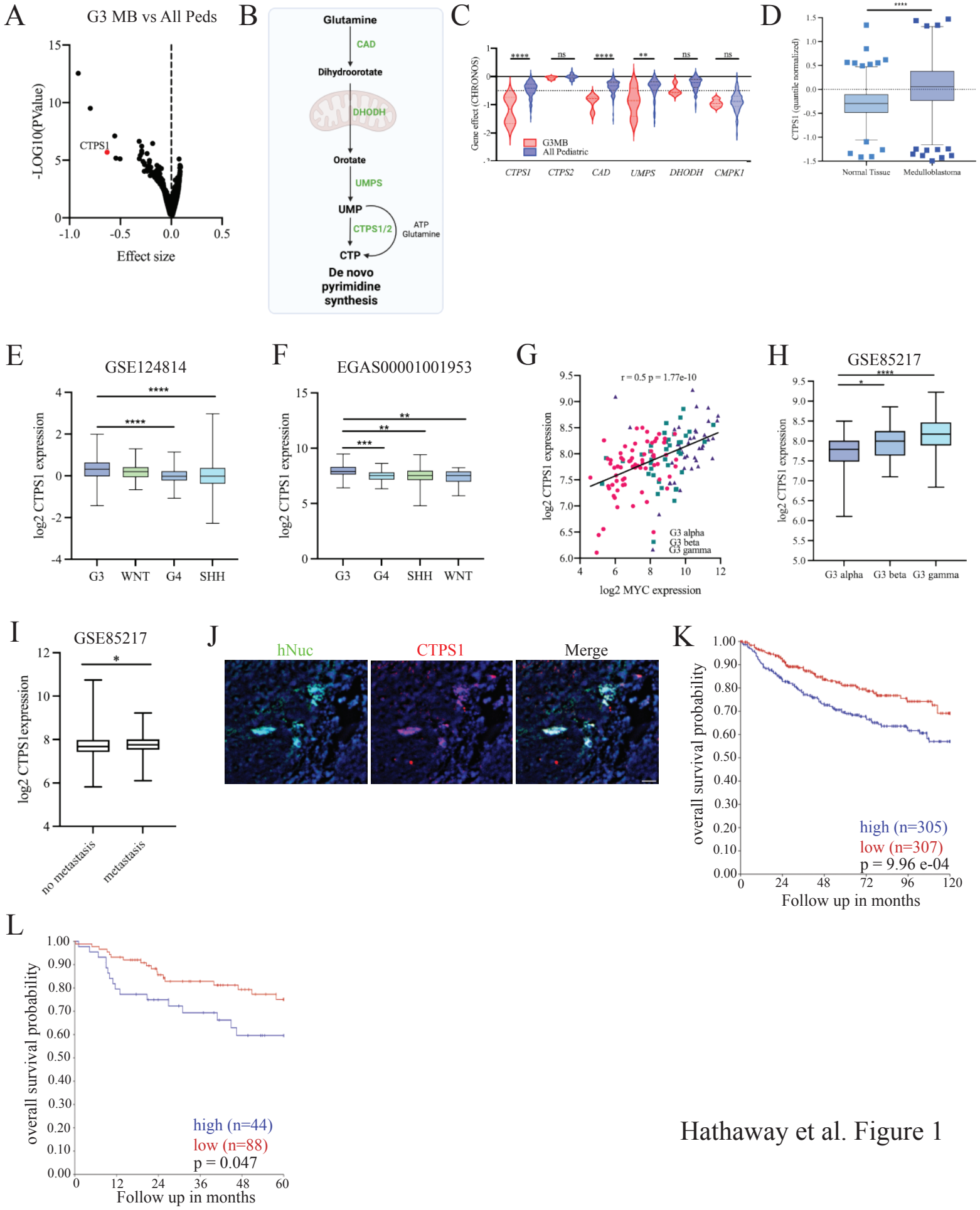

Hathaway et al. Figure 1

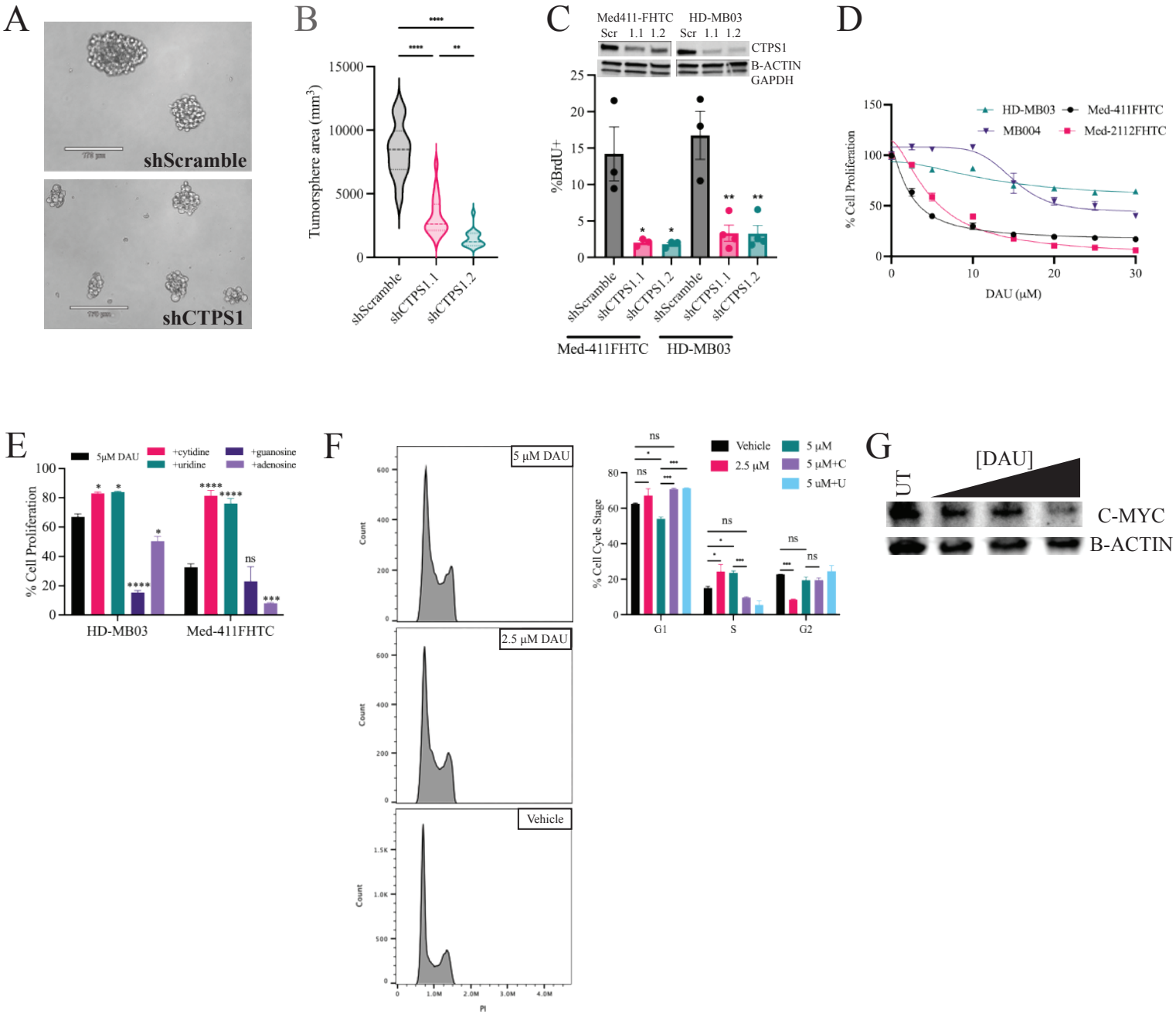

Hathaway et al. Figure 2

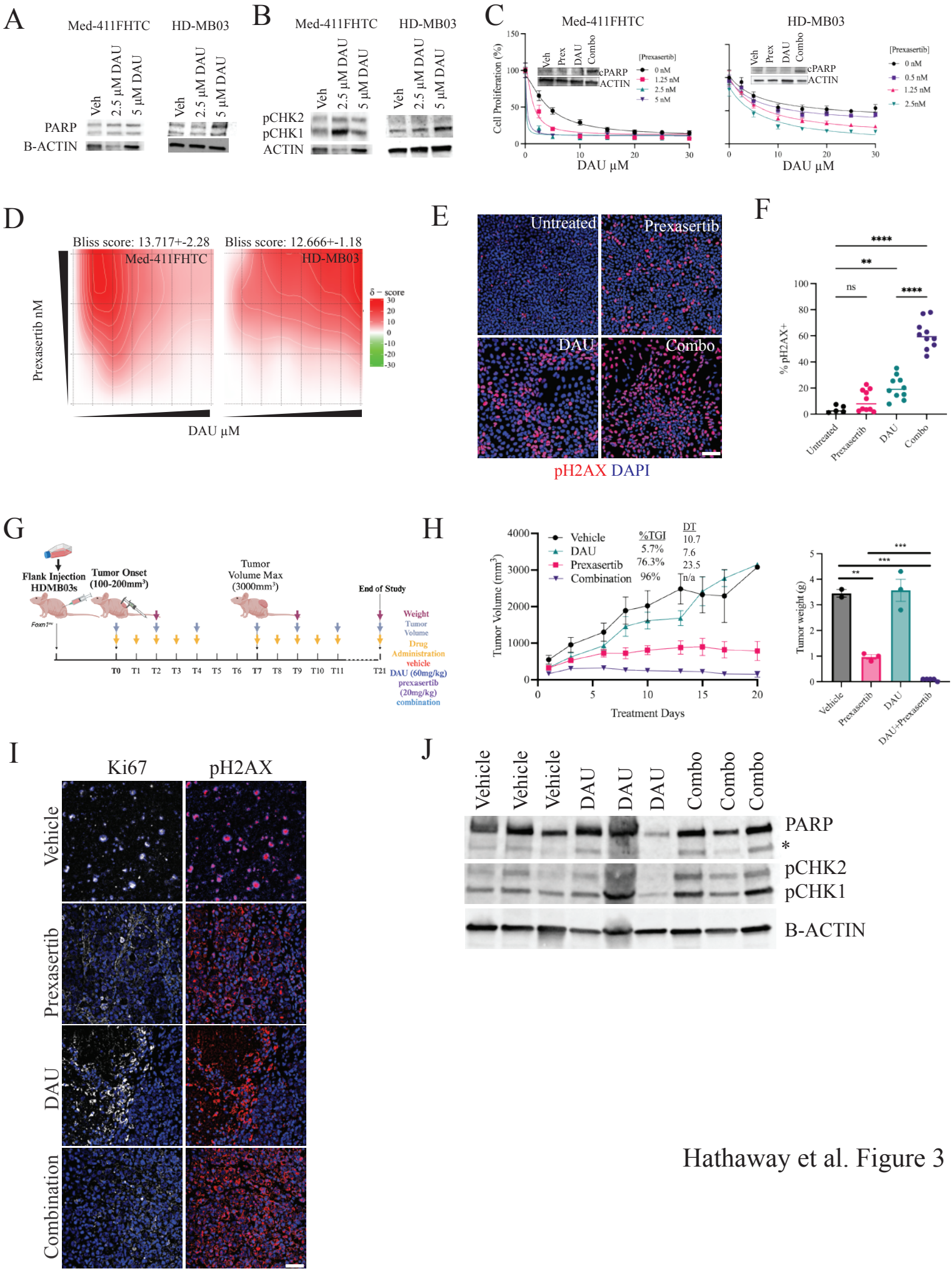

Hathaway et al. Figure 3

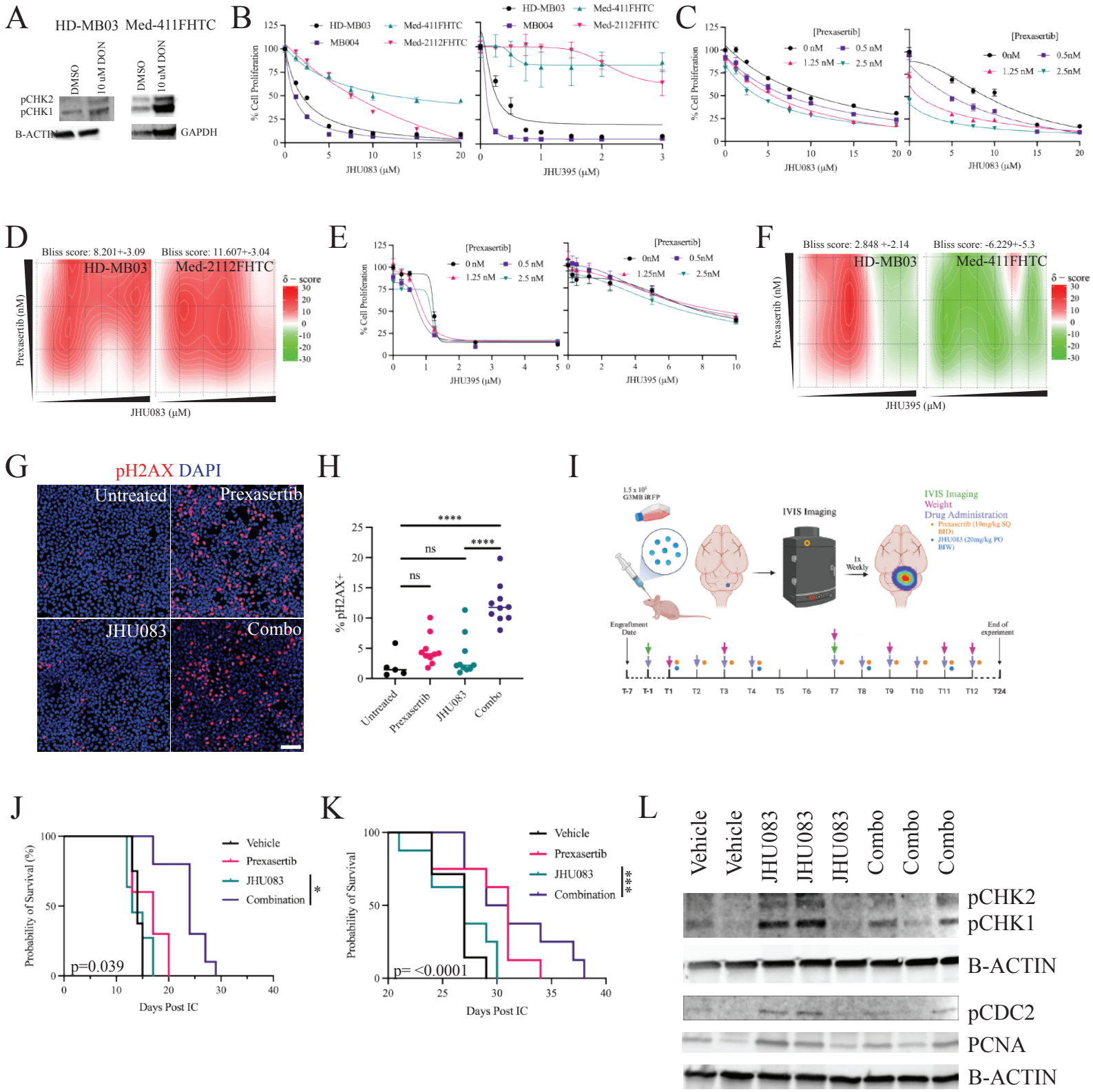

Hathaway et al. Figure 4

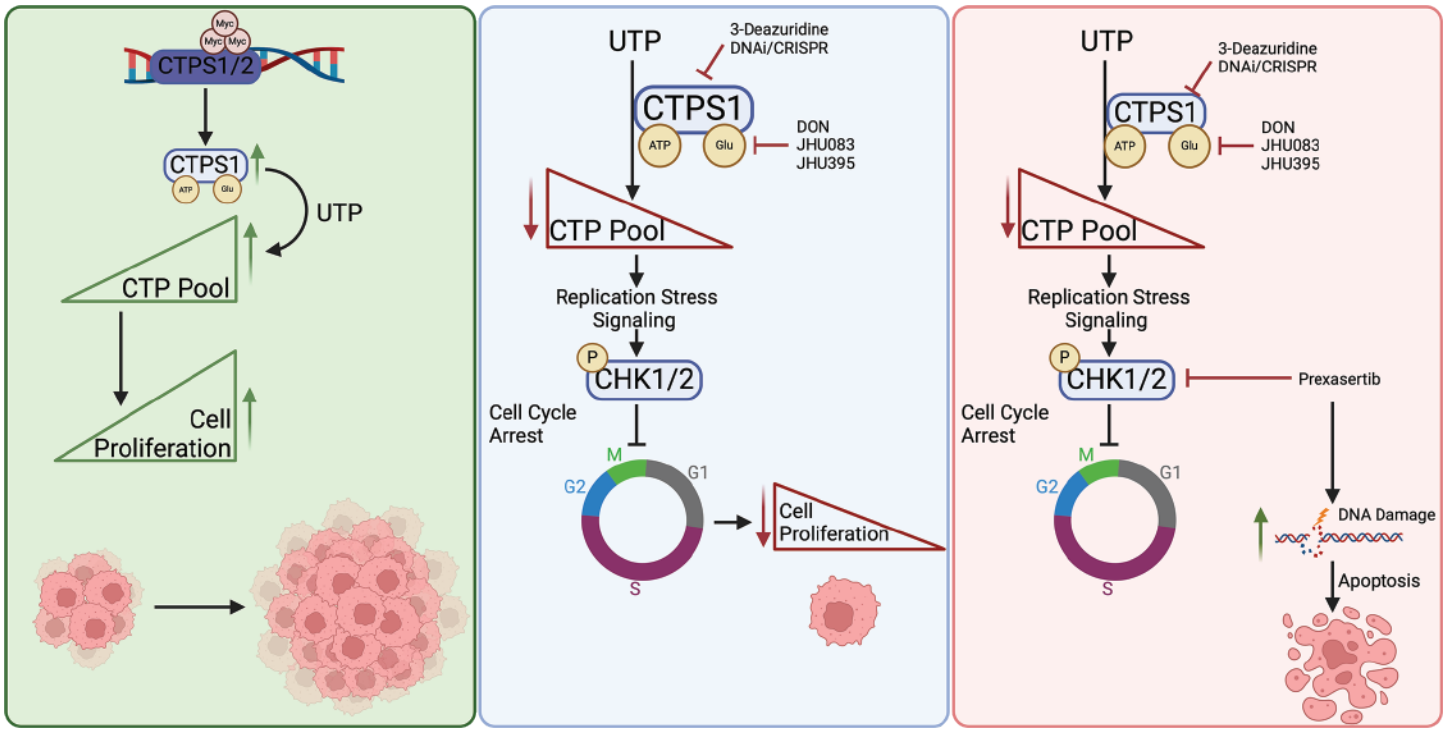

Hathaway et al. Figure 5

Table 1: Synergy scores for CTPS1 inhibitiors with prexasertib

	Drug 1	Drug 2	ZIP_synergy	ZIP_synergy_p_value	HSA_synergy	HSA_synergy_p_value	Loewe_synergy	Loewe_synergy_p_value	Bliss_synergy	Bliss_synergy_p_value
HD-MB03	prexasertib	DAU	12.60639662	5.33E-20	17.40683667	3E-117	10.83592936	0.000055	12.0364247	6.25E-15
	prexasertib	JHU395	5.489365734	0.000469	8.794607635	2.34E-08	-1.769786284	0.886	5.237058489	0.00347
	prexasertib	JHU083	6.122734406	0.0211	12.55551008	8.69E-21	9.364874489	0.000188	5.965281089	0.027
Med-411FHTC	prexasertib	DAU	11.03533493	4.03E-19	13.89670691	2.03E-92	8.049172603	0.101	10.78442356	2.35E-14
	prexasertib	JHU395	-1.533340467	0.655	-4.356167358	0.0353	-7.164625504	0.172	-3.25086577	0.396
	prexasertib	JHU083	8.805722263	0.0000897	18.33827545	6.16E-18	4.763895713	0.534	8.852162691	0.0000665